Journal of the Mechanics and Physics of Solids 118 (2018) 40–57

Contents lists available at ScienceDirect

Journal of the Mechanics and Physics of Solids

journal homepage: www.elsevier.com/locate/jmps

Spontaneous buckling-driven periodic delamination of thin films on soft substrates under large compression

Qiuting Zhang, Jie Yin*

Applied Mechanics of Materials Laboratory, Department of Mechanical Engineering, Temple University, 1947 North 12th Street, Philadelphia, PA 19122, USA

ARTICLE INFO

Article history:
Received 10 April 2018
Revised 5 May 2018
Accepted 11 May 2018
Available online 12 May 2018

Keywords:
Film-substrate system
Periodic buckle-delamination
Post-buckling
Interfacial toughness
Stretchability

ABSTRACT

Through a combination of experiments, theoretical modeling, and finite element simulation, we explore the mechanics governing the formation and evolution of periodic buckle-delamination on both micro- and macro-scale by bonding a thin film to an extremely pre-strained soft elastomeric substrate over 400%. We find that upon the large substrate pre-strain release, the deformation in the film follows a three-stage deformation regime, i.e. onset of localized blisters (Stage I), growth through delamination crack propagation to form periodic sinusoidal blisters (Stage II), and transition to post-buckled jig-saw-like blisters under fixed-end compression after crack arrest (Stage III). Related energy-based mechanics models on predicting the evolution and geometry of periodic blisters under moderate and large compression are developed and validated through both experiments and finite element simulation. Finally, we discuss the potential applications of harnessing spontaneous buckle-delamination for interfacial toughness measurement through the metrology of blisters, as well as design of extremely stretchable electronics by achieving an extremely lower value of maximum tensile strain in the buckle-delaminated film.

1. Introduction

Buckling instability, the transition from a flat surface to a wavy one under some form of critical load (Timoshenko and Gere, 1961), has historically been viewed as a failure mechanism in thin film-substrate systems. Over the past decade, the incredible potential of controllable buckling has been realized and harnessed in soft materials at small scales for broad applications, including surface micro-patterning (Bowden et al., 1998), thin film metrology (Chung et al., 2011), stretchable electronics (Khang et al., 2006; Rogers et al., 2010; Yao and Zhu, 2015), anti-biofouling (Efimenko et al., 2009), identity tags (Bae et al., 2015; Yin and Boyce, 2015), smart window (Lee et al., 2014, 2010; Lin et al., 2017), as well as tunable wetting, adhesion, acoustic, and optical properties (Ohzono et al., 2013; Rahmawan et al., 2014; Rudykh and Boyce, 2014; Saif, 2000). Generally, depending on the interfacial bonding strength in the film-substrate system, there are two typical modes of buckling instability, namely, wrinkling and buckle-delamination. Under strong interfacial bonding, wrinkling is preferred under compression, and thin films coherently deform with soft substrates. With small compressive strain in the film, the initially flat surface becomes buckled into periodic sinusoidal-shaped wrinkles over large areas. Further compression results in post-buckling behaviors such as period-doubling wrinkles, folds, localized ridges, and coexistence of different modes

* Corresponding author.
E-mail address: jieyin@temple.edu (J. Yin).

https://doi.org/10.1016/j.jmps.2018.05.009
0022-5096/

(Wang and Zhao, 2015). However, for relatively weak interfacial adhesion, buckling-driven delamination is preferred to occur with localized debonding of the thin film from substrates.

Unlike the demonstrated broad applications of wrinkling, harnessing buckling driven delamination for functionality is largely hindered by their localized characteristics, as often observed in the form of circular, straight, or telephone cord blister in buckling of thin films on stiff substrates (Hutchinson et al., 1992; Jensen and Sheinman, 2001; Moon et al., 2002; Ortiz and Gioia, 1994), as well as coexistence of wrinkles and buckle-delamination of thin films on soft substrates (Mei et al., 2007). To overcome the limitation, recently, there are growing research interest in buckling driven delamination of thin films or ribbons on extremely pre-strained soft elastomers. Recent studies have shown that periodic buckling-driven delaminated patterns over large areas can be formed either through constrained buckling by pre-patterning substrates with adhesive sites (Sun et al., 2006), where the ribbon delaminates between non-adhesive spots with controllable periodicity and buckle amplitude, or through freely buckling without prescribed adhesion spots by spontaneously choosing the energetically minimized buckle-delaminated geometries (Thomas et al., 2015; Zang et al., 2013, 2017). Such periodic buckle-delaminated patterns over large areas can enable multifunctionality in extreme stretchability, tunable superhydrophobicity, and large optical transmittance modulation range via mechanical strain, showing the promise of periodic buckle-delamination.

Compared to wrinkling and constrained delamination with pre-patterned adhesion sites, spontaneous and free buckle-delamination has several merits. First, one of the great advantages of buckling driven delamination is their high aspect ratio of buckles (defined as the ratio of buckle/wrinkle amplitude to wavelength), which is more than 10 times higher than that of previously reported shallow wrinkles (Chen and Crosby, 2014). The large surface roughness and high local curvature at both peak and valleys of delaminated buckles have the great potential to impact many fields, including surface topographies related properties such as adhesion, wetting, friction, and optics, as well as to augment the extreme stretchability in stretchable optical and electronic devices (Ebata et al., 2012). Second, compared to the constrained buckle-delamination, the spontaneously and freely buckling driven delamination is simple and does not require the complex procedure of lithographically defined surface adhesion sites. Furthermore, the strain energy can potentially be far more effectively released through both buckling and delamination, thus enabling a potential higher level of stretchability.

While there have been extensive studies on the mechanism of wrinkling of thin films on compliant substrates (Audoly and Boudaoud, 2008; Breid and Crosby, 2011; Cai et al., 2011; Chen and Hutchinson, 2004; Huang and Suo, 2002; Huang et al., 2005; Yin et al., 2009) and localized buckling-driven delamination of thin film on stiff substrates(Audoly, 1999; Hutchinson and Suo, 1992; Moon, 2013; Ortiz and Gioia, 1994, 1997) through both experimental and theoretical approaches, the mechanics of buckling-driven spontaneous periodic delamination of thin films on soft substrates remains largely unexplored under large deformation regime. Vella et al. (2009) explored the mechanics of macroscopic delamination of thin films on elastomers under small compression strain and proposed the scaling law of delamination periodicity, as well as its potential implication in stretchable electronics. Mei et al. (2011) studied the co-existence and co-evolution of periodic wrinkling and localized buckle-delamination of thin films on soft substrates under small deformation. However, a systematic investigation on the quantitative mechanics of the whole spontaneously periodic buckle-delamination process remains to be unrevealed crossing from small to large compression strain.

In this paper, we combine the experimental, theoretical, and numerical approach to explore the formation and evolution of spontaneously buckling-driven periodic delamination of thin films on extremely pre-strained elastomers over 400%, as well as to quantify the underlying deformation mechanism. This paper is organized as below: in Section 2, we present the experimental results on the whole deformation process of spontaneous buckle-delamination with the increase of large compression strain on both macroscopic and microscale. We find that depending on the magnitude of the compression strain, the deformation process can be classified as three stages, i.e. from the onset of buckle-delamination under small compression (Stage I), to growth of delamination cracks under moderate compression (Stage II), and to post-buckling after delamination arrest under large compression (Stage III). In Section 3, to quantitatively understand the evolution of delaminated buckles with the compression strain, we combine both geometric and energy-based mechanics models to predict the buckle-delaminated geometries at different deformation stages and compare with the experiment. In Section 4, we then conduct parametric numerical simulations using cohesive element modeling to investigate the role of interfacial toughness in determining the buckling mode and buckled geometry. Finally, in Sections 5 and 6, we discuss the potential applications of spontaneous buckle-delamination in interfacial toughness measurement and design of stretchable electronics.

2. Experimental results

Similar to wrinkling through the approach of substrate pre-stretching (Jiang et al., 2007), the generation of one-dimensional (1-D) periodic buckle-delaminated patterns is schematically illustrated in Fig. 1 by following 2 steps. In step 1, a thin sheet of elastomeric substrate with length L_o is first uni-axially pre-stretched to a large strain ε_{pre} over 100% to a new length L with $L = L_o\ (1+\varepsilon_{pre})$ (Fig. 1(i)), followed by bonding a stress-free thin film with length of L to the pre-strained substrate (Fig. 1(ii)). Here, we consider the pre-stretched state as a reference state for the film-substrate system. In step 2, the pre-strain in the substrate is gradually and fully released to compress the bonded film to make it spontaneously buckle and delaminate from the substrate (Fig. 1(iii)), thus generating 1-D periodic buckle-delaminated pattern (Fig. 1(iv–v)). We refer the strain-releasing state to be a compression process in the film. The compression strain ε for the film can be calculated as the ratio of reduced end-to-end displacement ΔL to the reference state of its length L as illustrated in Fig. 1(iv), i.e.

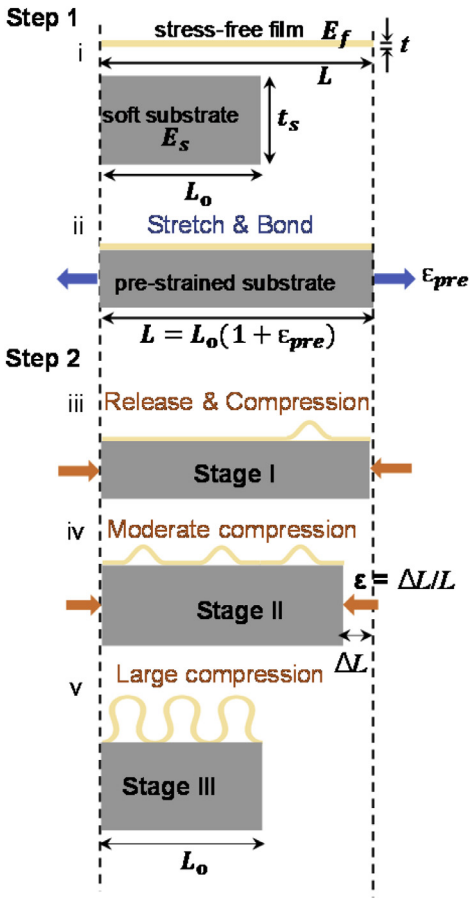

Fig. 1. Schematic illustration of generating spontaneous buckling-driven periodic delamination of thin film on pre-stretched elastomeric substrate through two sequential steps.

$$\varepsilon \equiv \frac{\Delta L}{L} \text{ with } \varepsilon \in [0, \varepsilon_{pre}/(1+\varepsilon_{pre})] \tag{1}$$

where ε will increase from 0 to ε_{pre} / $(1+\varepsilon_{pre})$ before and after full substrate pre-strain release, respectively.

2.1. Microscale spontaneous periodic buckle-delamination

We use the ion beam-based sputter coating system to produce continuous and ultrathin metal coatings with high resolution. At room temperature, we deposit a thin gold (Au) film (thickness $t = 40$ nm) on a uni-axially pre-stretched polydimethylsiloxane (PDMS) substrate (thickness $t_s = 2$ mm) with $\varepsilon_{pre} = 80\%$ using a model 681 Gatan high resolution ion beam coater with a base pressure of 1×10^{-6} torr. To evaluate the evolution of micro-scale buckle-delamination with the released strain, we use the scanning electron microscope (SEM) to in-situ characterize the delamination process of the buckled surface morphology.

Fig. 2a shows the tilted 45° SEM images of the sequential buckling and delamination process of the Au film on PDMS substrate during full release of the pre-strain. We observe that similar to wrinkling, spontaneous buckle-delamination also exhibits periodic characteristics with nearly uniform wavelength and amplitude of delaminated buckles or blisters. However, unlike the simultaneous formation of large-area periodic wrinkles, the buckle-delamination shows a sequential process from a localized delaminated pattern to a global periodic one with the increase of the released strain. The top-right of each image is the magnitude of the corresponding equivalent compression strain ε defined in Eq. (1). For a substrate pre-strain of $\varepsilon_{pre} = 80\%$, ε will increase from 0 before release to 44.4% after full release. Fig. 2a(i) shows the onset of localized buckle-delamination at a critical strain of $\varepsilon = 4.3\%$, where the buckled Au film locally debonds from the substrate, as evidenced by the exposed cross section of Au film from the cracked space. The crack is formed due to the Poisson's effect induced tensioning of the substrate in the transverse direction. The average delamination width δ and height h of the localized blisters are about 0.9 μm and 0.5 μm, respectively. The region between the localized blisters remains almost unbuckled and flat with their distance being about 10 times larger than the width of blisters. To evaluate the global periodicity of the

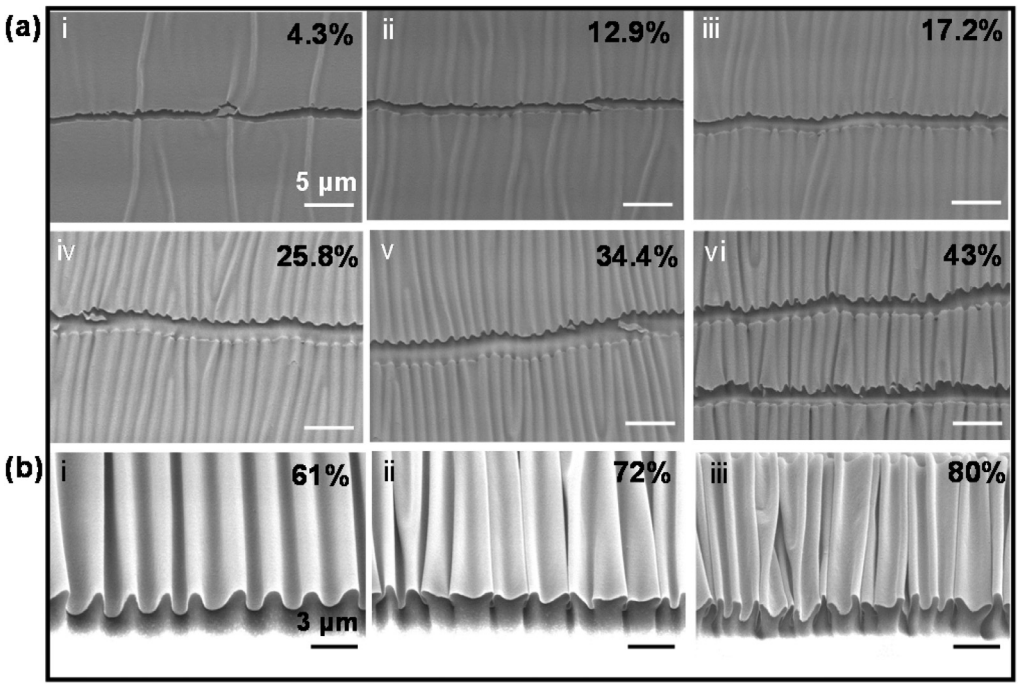

Fig. 2. Microscale periodic buckle-delamination experiments. (a) SEM images of evolution of buckle-delaminated Au films ($t = 40$ nm) on a PDMS substrate ($\varepsilon_{\text{pre}} = 80\%$) during the pre-strain release. (b) SEM images of buckle-delaminated Au films ($t = 40$ nm) on a 400% pre-strained silicone rubber substrate during the pre-strain release. Top-right corner in each image shows the corresponding equivalent compression strain in the substrate.

spontaneous buckle-delamination, we define the blister density as the number of blisters per 100 μm in the sample. It shows a blister density of about 21 $(100\,\mu\text{m})^{-1}$ at the onset of buckle-delamination. Upon further release, more number of new blisters occurs sequentially in the originally unbuckled regions. The blister density increases from about 21 to 83 $(100\,\mu\text{m})^{-1}$ at $\varepsilon = 25.8\%$, then it becomes saturated and the number of blisters remains unchanged as ε further increases, forming a globally periodic buckle-delaminated pattern with sinusoidal cross-sectional profiles.

To further explore the buckling-driven delamination under extremely large pre-strain, we replace the PDMS substrate with a more stretchable silicone rubber (thickness about 2 mm) and dramatically increase the substrate pre-strain ε_{pre} to 450%, while the Au film is kept as the same thickness of 40 nm. Correspondingly, the maximum compression strain ε will increase from 44.4% for $\varepsilon_{pre} = 80\%$ to 81.8% for $\varepsilon_{pre} = 450\%$ when the extreme pre-strain is fully released, which leads to a more complex buckle-delaminated pattern. Similarly, we observe the transition from sequential generation of localized buckle-delaminated blisters to formation of a globally periodic buckle-delaminated pattern with a saturated number of sinusoidal blisters. However, we find that when the large compression strain ε further increases over 50%, the sinusoidal profile transits to a jigsaw-like shape with wavelength of about 2.2 μm as shown in Fig. 2b(i) on the magnified view of the SEM image of the periodic buckle-delaminated profile at $\varepsilon = 61\%$. Further increase of ε leads to the debonding of wave troughs between two neighboring delaminated buckles, thus form the period-doubling of the delaminated buckles by combing two blisters into a big one with a wavelength of about 4.2 μm to release the strain energy more effectively. Similar phenomenon of period-doubling of wrinkles without debonding is reported before (Brau et al., 2010). However, to our knowledge, the current study presents the first experimental observation of period-doubling of delaminated buckles. Further compression leads to the post-buckling of two small buckles in a period-doubling buckle into smaller jigsaw-like shaped buckles with a wavelength of about 1.5 μm.

2.2. Macroscale spontaneous periodic buckle-delamination

To better understand and visualize the formation and evolution of the buckling driven 1-D periodic delamination, we also evaluate the spontaneous buckle-delamination of thin films on soft substrates on the macroscopic scale. In the macroscopic experimental setup, silicone rubber strips (thickness $t_s = 2$ mm) and 3 M scotch magic tapes (thickness $t = 50$ μm) are used to construct the soft substrates and thin films, respectively. The Young's modulus of the film and substrate is measured to be $E_f = 1.6$ GPa and $E_s = 0.5$ MPa, respectively. We use the Instron microtester (Model 5944) to pre-stretch the silicone rubber to a large strain of 400% with both ends clamped, i.e. $\varepsilon_{pre} = 400\%$, followed by attaching the 3 M adhesive tape to the central part of the stretched silicone rubber. To reduce the boundary effect, the length of the tape is set to be much smaller than that of the stretched silicone rubber. By slowly releasing the pre-strain with a compression rate of 10 mm/min controlled by

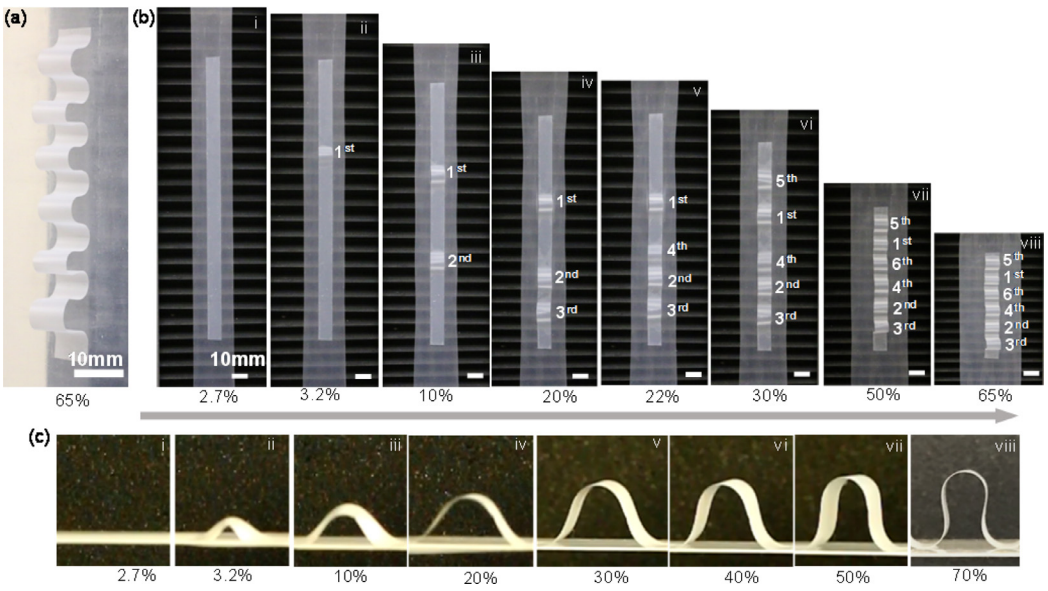

Fig. 3. Macroscopic periodic buckle-delamination of a thin polymeric tape film on 400% pre-strained silicone rubber. (a) The buckle-delaminated tape under a compression strain of 65%. (b) The corresponding delamination process with the increase of the applied compression strain (c) The profile evolution of a representative blister with the applied compression strain.

the microtester, the formation and evolution of the delaminated buckles can be examined and quantified. For $\varepsilon_{pre} = 400\%$, the compression strain ε will increase from 0 to 80% during the whole strain release process.

Fig. 3a shows the side-view optical image of the buckle-delaminated profile after full release of $\varepsilon_{pre} = 400\%$ (equivalent compression strain $\varepsilon = 80\%$). Similar to micro-scale delamination in Fig. 2, the buckle-delaminated profile exhibits periodic characteristics in both wavelength and amplitude of delaminated buckles, i.e. blisters. The evolution of the buckle-delamination process with the compression strain ε is shown in Fig. 3b. It shows that similar to micro-scale delamination, the macroscopic buckling driven delamination is a sequential process, where the blisters occur one by one with the increase of compression strain. The similar phenomenon is reported by Vella et al. (2009). Further increase of the strain does not generate new blisters and finally the number of blisters saturates to form a nearly uniformly periodic delaminated pattern, which is also similar to the observation on the micro-scale delamination in Fig. 2. Fig. 3c shows the side-view of corresponding geometrical shape evolution of a typical blister with the compression strain. It shows that throughout the whole releasing and compression process, the height of the blister keeps increasing with ε, while the delamination width of the blister first grows, then followed by a decrease with further compression. Finally, the initial sinusoidal profile of the blister transits into a jigsaw-like shape.

To quantify the shape of the blisters, we measure the evolution of their width δ and height h o with the compression strain ε as shown in Fig. 4. The onset of the first buckle-delaminated blister occurs at $\varepsilon \approx 3.6\%$, showing a dimension of $\delta \approx 10.5$ mm and $h \approx 3$ mm. As ε increases, δ increases monotonically and nonlinearly first until it arrives at a maximum value of $\delta \approx 22.5$ mm at $\varepsilon \approx 30\%$, then it drops approximately linearly with further increase of ε. In contrast, during the whole releasing and compression process, the height h of the blisters increases monotonically and nonlinearly with ε from $h \approx 3$ mm at $\varepsilon \approx 3.6\%$ to $h \approx 16$ mm at $\varepsilon \approx 75\%$.

From Fig. 4, we can classify the whole delamination process under large compression as three deformation stages: Stage I is the onset of buckling driven delamination before arriving at the critical buckling strain (left region highlighted by the light green-shaded area). Stage II is the growth and propagation of buckle-delamination (middle region highlighted by the light blue-shaded area). In Stage II, the delamination crack grows with the compression strain due to the large energy release rate. The deflection of delaminated thin film takes an approximate sinusoidal profile. As the compression strain further increases, both height and width will increase. The cracks at the interface open larger and crack tips propagate by de-adhering the interface. Stage III is an Euler buckling process of the delaminated blisters with both ends fixed to the substrate (right region highlighted by the light pink-shaded area), where the delaminated profile transits from a sinusoidal to a jigsaw-like shape. In Stage III, the delamination becomes arrested when the energy release rate drops below the interface toughness. The opening angle of the crack tips remains the same value upon further compression instead of growing. Cracks stop propagating, which indicates that the ends of the blisters are fixed to the surface of the substrate. Further compression leads to the decrease in the width of the blisters. Such experimental results will provide important information to guide the development of theoretical modeling discussed in Section 3.

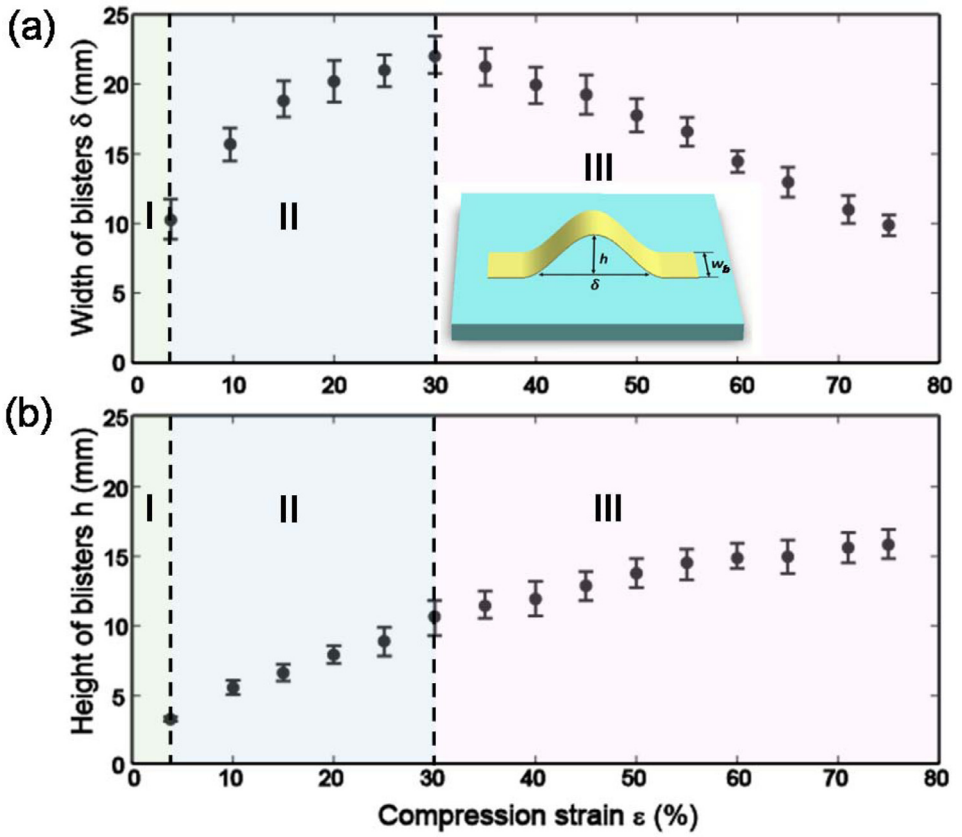

Fig. 4. The measured width (a) and height (b) of the blister as a function of the compression strain in the macroscopic buckle-delamination experiment, showing three deformation stages separated by dashed lines, Stage I (left region), Stage II (middle region), and Stage III (right region). The inset in (a) shows the schematic illustration of the blister width and height. (For interpretation of the references to color in this figure legend, the reader is referred to the web version of this article.)

3. Theoretical analysis and experimental examination

3.1. Onset of blisters in Stage I

The onset of localized buckle-delamination in thin films on soft substrate has been well studied before (Mei et al., 2011). Normally the initiation of localized delaminated blisters is induced from wrinkling instability. As the compressive strain in the film increases, the wrinkle amplitude grows, thus, delamination may occur due to the increase of both normal and shear tractions along the interface. For localized delamination of thin films on soft substrates, the critical strain ε_c for the onset of localized buckling driven blisters is given by (Mei et al., 2011)

$$\varepsilon_c = \varepsilon_{cw} + \alpha\left(\frac{\sigma_{\max}}{E_s}\right)^2 \tag{2}$$

where $\alpha = (3-4\nu_s)^2/[16(1-\nu_s)^4]$ can be estimated as $\alpha = 1$ for a soft substrate with its Poisson ratio ν_s approaching 0.5. $\varepsilon_{cw} = (3\bar{E}_s/\bar{E}_f)^{2/3}/4$ is the critical wrinkling strain (Chen and Hutchinson, 2004)"?>) with $\bar{E}_f = E_f/(1-\nu_f^2)$ and $\bar{E}_s = E_s/(1-\nu_s^2)$ being the plane-strain modulus of the thin film and substrate, respectively. $\sigma_{\max}$ is the maximum stress for the normal traction separation, which is known as the interfacial strength. In our macroscopic experiment, the critical wrinkling strain can be predicted as $\varepsilon_{cw} = 0.27\%$ with $E_f = 1.6$ GPa and $E_s = 0.5$ MPa ($\bar{E}_s/\bar{E}_f = 6 \times 10^{-4}$). The interfacial strength is measured to be about 0.91 MPa from the peel off test. From Eq. (2), the critical strain for localized buckle-delamination can be predicted as $\varepsilon_c = 3.12\%$, which agrees well with our experimental result on the strain of $\varepsilon_c = 3.6\%$ for the onset of localized blisters formation. We note that the critical buckling strain for localized delamination is over 10 times larger than that of the critical wrinkling strain, which is consistent with the previous report (Mei et al., 2011).

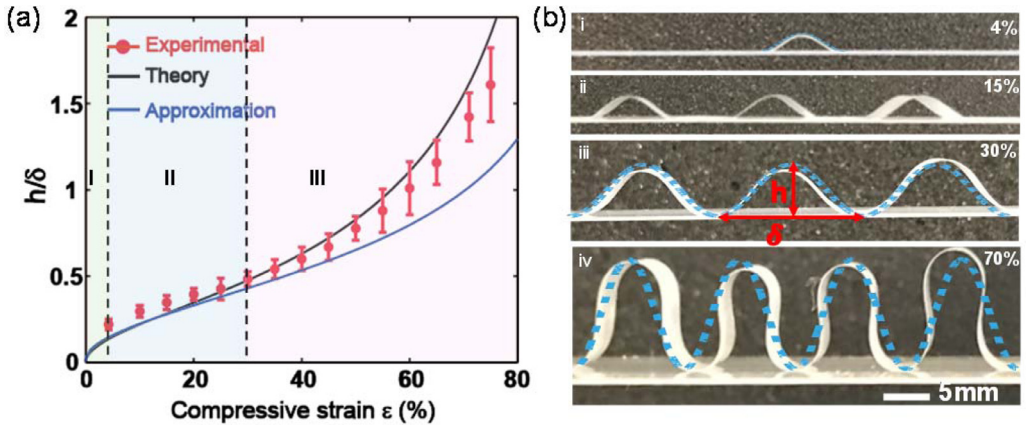

Fig. 5. Geometric modeling on the shape of blisters during compression. (a) Comparison of the evolution of aspect ratio of blisters (h/δ) as a function of compression strain ε between theoretical geometrical model (Eq. (5)), reduced approximate model (Eq. (6)), and the macroscopic buckle-delamination experiments. (b) The cross-sectional view of evolution of blisters with the compression strain during the macroscopic buckle-delamination. The dashed blue lines are the theoretically predicted sinusoidal-shaped profiles. (For interpretation of the references to color in this figure legend, the reader is referred to the web version of this article.)

3.2. Geometric model in Stage II

To further understand the evolution of blisters, we propose a theoretical model to quantitatively predict the size of blisters evolving with the compression strain. From the experimental observation, the geometry of periodic blisters with width δ and height h can be characterized by a sinusoidal profile under small and moderate compressive strain, i.e.

$$w = \frac{h}{2}\left[1 + \cos\left(\frac{2\pi x}{\delta}\right)\right] \tag{3}$$

Here, we assume the film is inextensible and the membrane strain in the film is fully released to form the delaminated blisters. Therefore, we have the geometric relationship on the length of the sinusoidal blister before and after a compression strain of ε as below

$$\int_{-\frac{\delta}{2}}^{\frac{\delta}{2}} \sqrt{1 + (w')^2}\,dx = \frac{\delta}{1-\varepsilon} \tag{4}$$

After substitution of Eq. (3) into Eq. (4), the implicit relationship between the geometry of the blister and the applied compression strain ε can be given as

$$\left(1 + \frac{\pi^2 h^2}{\delta^2}\right)^{\frac{1}{2}} E\left(\frac{\pi^2 h^2}{\delta^2 + \pi^2 h^2}\right) = \frac{\pi}{2(1-\varepsilon)} \tag{5}$$

where $E(\cdot)$ is the complete elliptic integral of the second kind. To simplify the analysis and get the explicit relationship between the aspect ratio of the blister (i.e. h/δ) and ε, Eq. (5) can be further approximated and reduced as

$$\frac{h}{\delta} \approx \frac{2}{\pi}\sqrt{\frac{\varepsilon}{1-\varepsilon}} \tag{6}$$

From Eq. (1), we know that $\varepsilon < 1$ for any magnitude of substrate pre-strain and thus Eq. (6) holds effective.

To validate the simple geometric model, we plot the aspect ratio h/δ as a function of ε and compare with the experimental measurements as shown in Fig. 5. Fig. 5a shows that the predicted h/δ in Eq. (5) (black curve) increases nonlinearly with the compression strain ε, which generally captures well with the trend in experiments, even for large compression strain in Stage III highlighted in light pink color-shaded area, while the reduced approximate model in Eq. (6) (blue curve) only agrees well with the experiment in the small and moderate compression strain ε in Stage I and Stage II and starts to dramatically deviate from both experiment and the model in Eq. (5) when ε is beyond about 30% in Stage III. We also observe that for both full and reduced models, a deviation between the experiment and theoretical prediction of h/δ is found when the compressive strain is relatively large, where the experimental measurements are lower than that of the theoretical prediction from Eq. (5). Such a disparity results from the shape changing of the blisters transiting from Stage II to Stage III. As we can see, in Fig. 5(b), when we overlap the geometrically predicted profiles (blue dashed lines) based on the sinusoidal assumption and Eq. (5) with the experimental profiles, we find that as ε increases, the sinusoidal shape fits well with the profile of the observed periodic delaminated blisters at moderate strain of $\varepsilon \leq 30\%$ in Stage II (Fig. 5i–iii), however, under large strain in Stage III, for example, at $\varepsilon = 70\%$, the calculated sinusoidal profile from the model does no longer match with

the jig-saw-like shaped blisters observed in the experiment (Fig. 5iv). We notice that the curvature on the top of the jig-saw-like blisters is much larger than that of the predicted sinusoidal shape. Despite the similar periodicity of δ, generally the predicted height of the sinusoidal blisters is higher than that of the observed jig-saw-like blisters on average, which is consistent with the predicted relatively higher magnitude of h/δ in Fig. 5a.

Thus, based on the above results of the simple geometric relation, we confirm that sinusoidal characterization of the delaminated blisters can only be used to describe the buckle-delaminated profile under small and moderate compression in Stage II. At large compression strain in Stage III, a different parametric function should be used for characterizing the jig-saw-like shape (discussed in Section 3.3). The two different profiles also represent two different deformation mechanism and mechanics models, which will be discussed in the following sections.

3.3. Energy-based mechanics modeling in Stage II and experimental validation

Despite the promise of predicting the aspect ratio of delaminated buckles from the simple geometrical model, the explicit respective expression for both delamination amplitude and width remains to be solved. Since the morphology of delaminated patterns is governed by the minimization of the potential energy (Gioia and Ortiz, 1997), the dimension parameters of blisters can be derived using the energetical approach. The thin film is modeled as an elastic thin plate and the substrate is modeled as a semi-infinite solid satisfying Neo-Hookean constitutive law to account for the large deformation in the silicone rubber substrate.

The total energy in the film-substrate system U_{total} consists of the stretching energy U_{str} and bending energy U_{bend} in the film, the elastic energy stored in the substrate U_{sub}, and the adhesion energy between the film and the substrate U_{adh}, i.e.

$$U_{total} = U_{str} + U_{bend} + U_{sub} + U_{adh} \tag{7}$$

where

$$U_{str} = \frac{1}{2}\int_s \sigma_{\alpha\beta}\varepsilon_{\alpha\beta} t dA \tag{8}$$

$$U_{bend} = \frac{1}{2}\int_s M_{\alpha\beta}\kappa_{\alpha\beta} dA \tag{9}$$

$$U_{sub} = \int_V W_s dV \tag{10}$$

$$U_{adh} = \int_s \Gamma dA \tag{11}$$

$\sigma_{\alpha\beta}$ and $\varepsilon_{\alpha\beta}$ are the membrane stress and membrane strain, respectively. $M_{\alpha\beta}$ and $\kappa_{\alpha\beta}$ are the bending moment and bending curvature, respectively. Each Greek subscript takes values 1 and 2 representing the in-plane axis x and y. W_s is the strain energy density. Γ is the interfacial toughness. We have

$$\sigma_{\alpha\beta} = \bar{E}_f\left[\left(1-\nu_f\right)\varepsilon_{\alpha\beta} + \nu_f\varepsilon_{\gamma\gamma}\delta_{\alpha\beta}\right] \tag{12}$$

$$\varepsilon_{\alpha\beta} = \varepsilon^0_{\alpha\beta} + \frac{1}{2}\left(u_{\alpha,\beta} + u_{\beta,\alpha}\right) + \frac{1}{2}w_{,\alpha}w_{,\beta} \tag{13}$$

$$M_{\alpha\beta} = D\left[\left(1-\nu_f\right)\kappa_{\alpha\beta} + \nu_f\kappa_{\gamma\gamma}\delta_{\alpha\beta}\right] \tag{14}$$

$$\kappa_{\alpha\beta} = -w_{,\alpha\beta} \tag{15}$$

$$W_s = \frac{E_s}{6(1-2\nu_s)}(J-1)^2 + \frac{E_s}{4(1+\nu_s)}(\bar{I}_1 - 3) \tag{16}$$

where $\delta_{\alpha\beta}=1$ when $\alpha=\beta$ otherwise $\delta_{\alpha\beta}=0$. $\varepsilon^0_{\alpha\beta}$ is the applied strain in the film. $w_{,\alpha} = \partial w/\partial x_\alpha$ and $u_{\alpha,\beta} = \partial u_\alpha/\partial x_\beta$, where u_1 and u_2 are the respective in-plane displacements along the coordinate x and y and w is the out-of-plane displacement of the film along z. $D=\bar{E}_f t^3/12$ is the bending stiffness. J is the determinant of deformation gradient and $\bar{I}_1$ is the first invariant of the deviatoric part of the left Cauchy-Green tensor. The membrane force $N_{\alpha\beta}$ is $N_{\alpha\beta}=\sigma_{\alpha\beta}\, t$. For the film-substrate interface, the equilibrium requires that the in-plane traction $T_\alpha = N_{\alpha\beta,\beta}$ and the out-of-plane traction $T_3 = -\bar{E}_f t^3 w_{,\alpha\alpha\beta\beta}/12 + (N_{\alpha\beta}w_{,\alpha})_{,\beta}$.

For 1-D straight-sided delaminated pattern observed in experiments, the profile of periodic blisters w can be assumed to take the approximate sinusoidal form in Eq. (3). The negligible shear stress at the film-substrate interface leads to a zero interfacial shear traction, i.e. $T_\alpha = N_{\alpha\beta,\ \beta}=0$, which gives the in-plane displacement taking the form of $u_1 = \frac{\pi h^2}{16\delta}\sin(4\pi x/\delta)$

and $u_2 = 0$ with the help of Eqs. (12) and (3) (Chen and Hutchinson, 2004). Thus, the stretching and bending energy in the film can be obtained after substituting Eqs. (12)–(15) into Eqs. (8) and (9), i.e.

$$U_{str} = \frac{1}{2}\int_{-\frac{\delta}{2}}^{\frac{\delta}{2}} \bar{E}_f t\left(\varepsilon - \frac{\pi^2 h^2}{4\delta^2}\right)^2 w_b dx = \frac{\bar{E}_f t\delta}{2}\left(\varepsilon - \frac{\pi^2 h^2}{4\delta^2}\right)^2 w_b \tag{17}$$

$$U_{bend} = \frac{1}{2}\int_{-\frac{\delta}{2}}^{\frac{\delta}{2}} \frac{\bar{E}_f t^3}{12}(w_{,11})^2 w_b dx = \frac{\pi^4 \bar{E}_f t^3 h^2}{12\delta^3} w_b \tag{18}$$

where w_b is the width of the film. $\varepsilon = \varepsilon_{11}^0$ is the magnitude of the applied compressive strain in the film. As discussed in the simple geometrical model in Section 3.2, the assumption of inextensible film works well for the delamination in Stage II as shown in Fig. 5a. From Eq. (6), we have the approximate relationship between the applied strain ε and the geometry of the blisters as $\varepsilon \approx \pi^2 h^2/4\delta^2$. Thus, in terms of Eq. (17), it gives $U_{str} \approx 0$, i.e. the stretching energy in the film in can be reasonably neglected with the validated inextensible assumption.

Next, we will discuss the strain energy in the substrate. The calculation of the strain energy in the Neo-Hookean substrate was discussed by Song *et al.*, through the perturbation analysis of the substrate (Song et al., 2008). As seen in the microscopic delamination of Au films on PDMS or silicone rubber substrates (Fig. 2), the top surface of the soft substrate also becomes periodically wrinkled despite the delamination of the coating, where the wrinkle amplitude h' is much shallower than that of the delaminated blisters while the wavelength is preserved. Thus, the out-of-plane displacement of the top surface of the substrate w_{sub} can be approximated as $w_{sub} = h'/2[1 + \cos(2\pi x/\delta)]$. By solving the force equilibrium equation under finite deformation with negligible shear force and displacement boundary conditions in the interface, the strain energy in the nonlinear elastic substrate can be given by (Song et al., 2008)

$$U_{sub} = \frac{\pi}{12}\frac{E_s h'^2}{1-\varepsilon}\left(1 + \frac{5\pi^2}{128}\frac{h'^2}{\delta^2}\right) w_b \tag{19}$$

Unlike the coherent deformation in the wrinkling of thin films bonded to soft substrates, the deformation in the substrate after delamination can be approximately considered as the elastic contact problem between a wavy "rigid" structure (i.e. the periodic blisters) and an elastic soft half-space within the small and finite deformation regime. For a single blister, the maximum contact pressure $p_{\max}$ can be obtained from the equilibrium on the film/substrate interface as

$$p_{\max} = (T_3)_{\max} \text{ with } T_3 = -\bar{E}_f t^3 w_{,\alpha\alpha\beta\beta}/12 + (\sigma_{\alpha\beta} t w_{,\alpha})_{,\beta} \tag{20}$$

After substituting Eqs. (3) and (12) into Eq. (20), $p_{\max}$ can be given by

$$p_{\max} = -\frac{\bar{E}_f t h}{2}\left(\frac{2\pi}{\delta}\right)^4\left[\frac{t^2}{12} + \left(\frac{\delta}{2\pi}\right)^2\left(\varepsilon - \frac{\pi^2 h^2}{4\delta^2}\right)\right] \approx -\frac{2}{3}\bar{E}_f t^3 h\left(\frac{\pi}{\delta}\right)^4 \tag{21}$$

By approximating the sinusoidal wave trough of a single blister in the film as a cylinder with the same radius curvature R as that of the trough, i.e. $R = \delta^2/2\pi^2 h$, the penetration depth in the substrate, i.e. the out-of-plane deflection h' can be estimated to scale with $h'/h \propto (t/\delta)^6(\bar{E}_f/\bar{E}_s)^2$. Thus, the ratio of the stored strain energy in the substrate U_{sub} and the bending energy in the film U_{bend} can be approximately estimated to scale with $U_{sub}/U_{bend} \propto (\bar{E}_f/\bar{E}_s)^3(t/\delta)^9$. For both macroscopic and microscopic delamination experiments shown in Figs. 2 and 3, t/δ is in the order of 10^{-3} while $\bar{E}_f/\bar{E}_s$ is in the order of 10^4 and 10^5 for tapes and Au coating on silicone rubber, respectively. Thus, for both cases, the strain energy in the substrate can be negligible when compared to that of the delaminated film. Accordingly, the effect of materials nonlinearity in the elastomeric substrate in influencing the buckle-delaminated morphology becomes negligible.

Therefore, the total potential energy in a delaminated blister per unit width can be further simplified as:

$$U_{total} = U_{bend} + U_{adh} = \frac{\pi^4 \bar{E}_f t^3 h^2}{12\delta^3} + \frac{\Gamma\delta}{1-\varepsilon} \tag{22}$$

Now the equilibrium profile of the blisters can be obtained by minimizing the total potential energy, i.e. the bending energy in the thin film and adhesion energy in the interface,

$$\frac{\partial U_{total}}{\partial \delta} = 0 \tag{23}$$

After canceling h in Eq. (23) in terms of the geometric relationship in Eq. (6), the width and amplitude of the periodic blisters in Stage II can be obtained as

$$\delta = \pi t\sqrt{\frac{\bar{E}_f t}{\Gamma}}\sqrt{\varepsilon} \tag{24}$$

$$h = 2\sqrt{\frac{\bar{E}_f t}{\Gamma}}\frac{\varepsilon}{\sqrt{1-\varepsilon}} \tag{25}$$

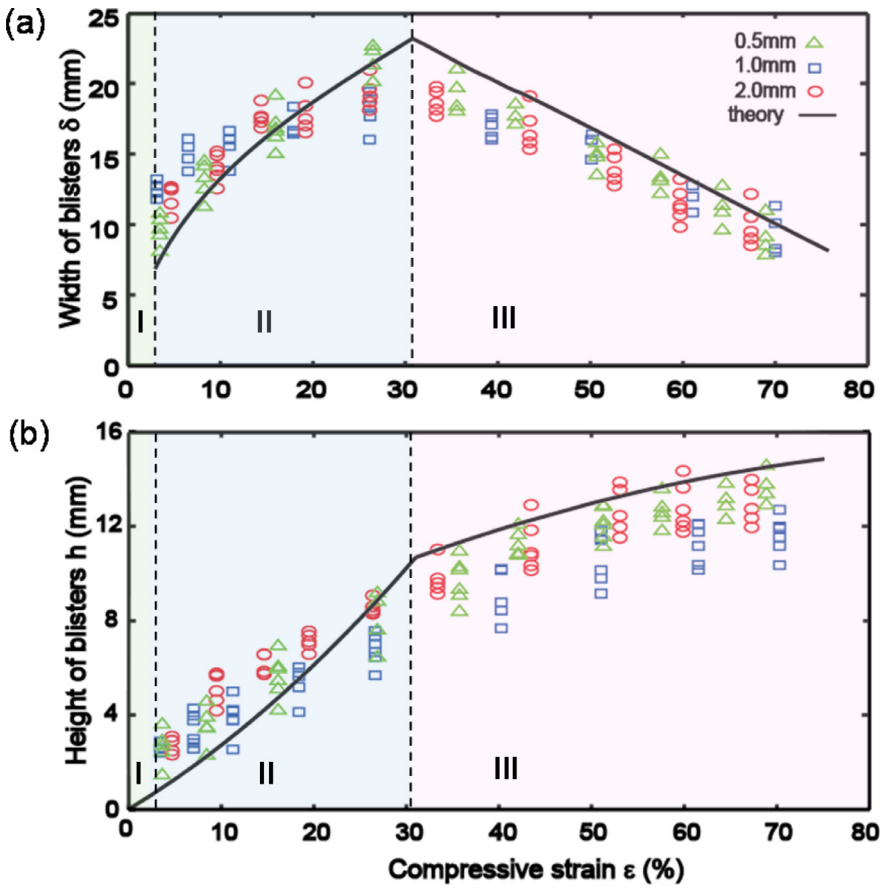

Fig. 6. Comparison between the theoretical model and experimental measurement of the blister width (a) and height (b) as a function of applied compressive strain ε in the macroscopic buckle-delamination experiment for tapes with different strip width for different deformation stages. The respective blister width and height are theoretically predicted by Eqs. (24) and (25) in Stage II, and by Eqs. (29) and (5) in Stage III. (For interpretation of the references to color in this figure legend, the reader is referred to the web version of this article.)

To validate the theory, we compare it with the macroscopic delamination experiment, where $E_f = 1.6\,\text{GPa}$ is the Young's modulus of the film tape, $t = 50\,\mu\text{m}$ is the thickness of the film, and $\Gamma \approx 1.5\,\text{J/m}^2$ is the interfacial toughness. Fig. 6 shows the comparison of the blister width δ and blister height h between the experimental measurement and theoretical prediction as a function of the compressed strain ε during Stage II for tapes with different width w_b. It shows that in Stage II, both δ and h increase nonlinearly with the applied strain ε, which agree well with the experiments (Fig. 6). We also note that both δ and h are approximately independent of the tape width.

3.4. Transition from Stage II to Stage III

As the crack propagates and the blisters grow, the delamination becomes arrested when the energy release rate drops below the interface toughness, thus the crack stops propagating, and the periodic blisters reach the maximum width $\delta_{\max}$. At this point, it defines a transition point from Stage II to Stage III at a critical applied strain defined as the transition strain ε_T. At the transition point, geometrically, $\delta_{\max}$, ε_T, the number of the periodic blisters n, and the length of the film L satisfy

$$n\delta_{\max} = L(1 - \varepsilon_T) \tag{26}$$

Thus, it gives

$$\varepsilon_T = 1 - \frac{n\delta_{\max}}{L} \tag{27}$$

Combining Eqs. (24) and (27), we have

$$\varepsilon_T = 1 + \frac{n^2\pi^2\bar{E}_f t^3}{2\Gamma L^2} - \sqrt{\left(\frac{n^2\pi^2\bar{E}_f t^3}{2\Gamma L^2}\right)^2 + \frac{n^2\pi^2\bar{E}_f t^3}{\Gamma L^2}} \tag{28}$$

For the macroscopic delamination experiment, we have $n=6$ and $L=200$ mm. Thus, the transition strain ε_T can be predicted from Eq. (28) as $\varepsilon_T=31\%$, which agrees well with the experimental measurement of the transition zone of 29%–32% as shown in Fig. 6a.

In Stage III, as the applied strain further increases beyond ε_T, the number of the periodic blisters n remains unchanged as observed from the experiment, while the width of the blisters starts to decrease with further compression of the strain due to the fixed ends of each blister. Thus, the blisters with two ends anchored to the substrate undergo a fixed end compression and their width will decrease proportionally with the applied compression strain ε in the substrate, i.e. the width of the blisters δ_{III} in Stage III is given as

$$\delta_{III}=\frac{\delta_{\max}}{1-\varepsilon_T}(1-\varepsilon) \tag{29}$$

Next, we compare the simple model in Eq. (29) with the experimental measurement in Stage III as shown in Fig. 6a. It shows that for all tapes with different widths of $w_b=0.5$, 1.0, and 2.0 mm, the simple model is consistent with the experimental measurement of the linear trend of the blister width vs. the applied strain.

Correspondingly, with Eq. (29), the theoretically predicted amplitude of the blisters h_{III} in Stage III can be obtained through the assumption of inextensional films by satisfying the geometrical relationship in Eq. (5). Fig. 6b shows that the theoretically predicted amplitude is slightly higher than the measured data on the amplitude of the blisters in Stage III. The reason for such a disparity is that we assume an idealized sinusoidal shape in the model for Stage III, which is different from the jigsaw-like shape observed in the experiment. Thus, theoretical models by considering the different deformed shape in Stage III are needed, which is discussed in the following section.

3.5. Modeling of jigsaw-like profile of blisters in Stage III

In Stage III, there is no more adhesion energy releasing between the interface. The deformation of a representative blister can be considered as bending of a beam with an end-to-end confinement under compression, an elastica problem (Humer and Irschik, 2011; Love, 1906; Wagner and Vella, 2013). The jigsaw-like profile is also an elastica curve. The analytical solution of its profile can be obtained through the energy minimization method. The total potential energy of the system only consists of the bending energy of thin film U_{bend} and the potential energy from the compressive force P loaded at the ends, i.e.

$$U_{total}=U_{bend}-P\Delta l \tag{30}$$

where Δl is the end-to-end displacement between two constraints. We define the profile of blisters as the rotation field of the stripe's axis $\theta(s)$, where $s\in[-\frac{l}{2},\frac{l}{2}]$ is the curvilinear coordinate and l is the constant arc length. The total potential energy can be written as

$$U_{total}=\frac{1}{2}\int_{-\frac{l}{2}}^{\frac{l}{2}}D\left[\theta'(s)\right]^2ds-P\int_{-\frac{l}{2}}^{\frac{l}{2}}[1-\cos\theta(s)]ds \tag{31}$$

where D is the bending stiffness of the film. By minimizing the energy i.e. $\frac{\partial U_{total}}{\partial s}=0$, we can get the governing equation as below

$$\theta''(s)+\alpha^2\theta(s)=0, s\in\left[-\tfrac{l}{2},\ -\tfrac{l}{4}\right] \tag{32}$$

with the boundary conditions $\theta(-\frac{l}{2})=0$ and $\theta'(-\frac{l}{4})=0$, where $\alpha=\sqrt{P/D+[\theta'(-\frac{l}{2})]^2/2}$ is a dimensionless parameter. By integrating the equilibrium equation in Eq. (32), the jig-saw-like or elastica profile in Stage III can be described as

$$\delta(s)=-s+\frac{2}{\alpha}\mathrm{E}\left[\mathrm{am}\left(\alpha s,\sin\left(\bar{\theta}/2\right)\right),\sin\left(\bar{\theta}/2\right)\right] \tag{33}$$

$$h(s)=\frac{2\sin\left(\bar{\theta}/2\right)}{\alpha}[1-\mathrm{cn}(\alpha s)] \tag{34}$$

where $\bar{\theta}=\theta(-\frac{l}{4})$, E(,) is the incomplete elliptic integrals of the second kind, am and cn are the Jacobi amplitude and the Jacobi cosine amplitude functions, respectively. The dimensionless load parameter α can be determined by the angle of rotation as

$$\alpha=\frac{4}{l(1-\varepsilon)}\left\{2\mathrm{E}\left[\mathrm{am}\left(\kappa\left(\sin\left(\bar{\theta}/2\right)\right),\sin\left(\bar{\theta}/2\right)\right),\sin\left(\bar{\theta}/2\right)\right]-\kappa\left(\sin\left(\bar{\theta}/2\right)\right)\right\} \tag{35}$$

where $\kappa()$ is the complete elliptic integral of the first kind.

Fig. 7a shows the evolution of the profile of the blisters calculated from Eqs. (33) and (34) for the tape film with the applied compressive strain ε in Stage III ($\varepsilon\geq 30\%$). It shows that as ε increases beyond the transition strain of about 30%, the predicted profile gradually transits from an approximately sinusoidal shape to an elastica shape. When ε reaches a critical value of 84%, the blister with the elastica shape will be self-contacted. To examine the model, we overlap the theoretically

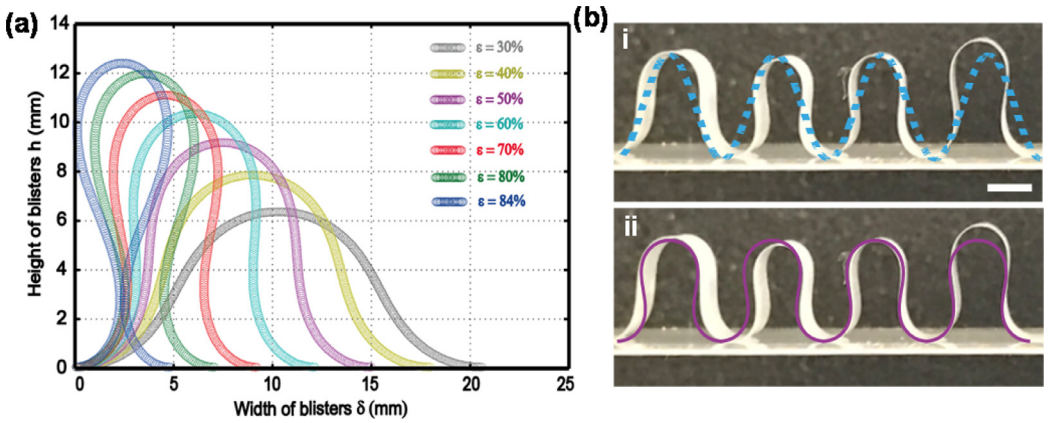

Fig. 7. (a) Theoretically predicted evolution of the cross-sectional profiles of blisters in Stage III as a function of applied compressive strain ε. (b) Overlapping of the predicted sinusoidal profile (i) and elastica profile (ii) with the macroscopic delamination experiment at $\varepsilon = 70\%$. Scale bar is 5 mm.

predicted profile at $\varepsilon = 70\%$ with the optical image of blisters observed in experiment under the same compressive strain of 70%, which shows an excellent fitting with the experimental profiles as shown in Fig. 7b(ii), while the predicted profile from the model by assuming sinusoidal shapes cannot fit well with the experiment despite the capture of similar amplitude and wavelength (Fig. 7b (i)).

4. Finite element modeling of periodic buckle-delamination

4.1. Simulation of delaminated blisters formation and evolution

Next, finite element method (FEM) is used to simulate the formation and evolution of delaminated blisters to validate the theoretical prediction discussed in Section 3. A dynamic explicit simulation is used to simulate the quasi-static process of the buckle-delamination. A tri-layer 2D model is built with a thin stiff film bonded to a soft elastomeric substrate and an adhesive layer is set in between. The thin film and substrate are fine meshed and modeled as 2D quadrilateral plane-strain elements. The tri-layer system is uniaxially compressed by controlling the applied displacement. The thin film, i.e. the tape in the macroscopic experiment is modeled as a linear elastic material with $E_f = 1.6$ GPa and $v_f = 0.2$. The silicone rubber substrate is modeled as a nonlinear hyperelastic Neo-Hookean material with $E_s = 0.5$ MPa and $v_s = 0.49$. The adhesive layer between the film and the substrate is modeled with a thin layer of 4-node 2D cohesive elements. Based on the traction-separation cohesive material law, an isotropic cohesive behavior is assumed. In the FEM model, the interfacial property is defined using cohesive zone model via the interfacial toughness Γ and the maximum traction stress $\sigma_{\max}$, which is known as the strengths of the interface. The displacement jump across the interface can be estimated as $\delta = \frac{\Gamma}{e\sigma_{\max}}$. Along the horizontal direction, the film-substrate system is compressed uniaxially to generate the buckle-delaminated blisters, where a linear buckling mode analysis is first conducted to extract the first 3 buckle eigenmode as the introduced geometric imperfection for the following post-buckling dynamic analysis. Considering the large difference between the elastic properties and the thickness of the film and the substrate, it remains challenging to simulate the evolution of blisters under large compression strain due to the large deformation and distortion of elements in the substrate. In this work, only a maximum compression strain of 35% is achieved to ensure the convergence of the simulation.

Fig. 8 shows the sequential formation and evolution of the buckle-delamination in the film-substrate system as the applied compression strain ε increases from 0 to 35%. It shows that when ε increases to a critical value of 4.1%, two small localized blisters occur simultaneously close to the two ends with concurrent much shallower periodic wrinkles in between (Fig. 8i), which defines the onset of localized blisters formation. Similar concurrent existence of wrinkles and delaminated buckles are reported before by Mei et al. (2011). The critical delamination strain from the simulation agrees well with that of $\varepsilon_c = 3.6\%$ observed in the experiment. As ε further increases to 8.5%, the 2nd two localized blisters occur simultaneously, which are away from the 1st two blisters, while the small wrinkles are smoothened (Fig. 8ii). More number of blisters occurs sequentially in between as ε further increases (Fig. 8iii–iv). However, when ε is increased beyond 18.7%, the number of blisters saturates at 7. Further increase of ε leads to the growth of the blisters in both width and amplitude (Fig. 8iv–vi), while the number of blisters remains unchanged to form a periodic distribution of the blisters at $\varepsilon = 35\%$. The whole buckle-delamination process from the FEM simulation is qualitatively consistent with the experimental observation in Fig. 3. Interestingly, similar distribution of non-uniform sizes among the blisters in the macroscopic experiment is also observed in the simulation (Fig. 8vi).

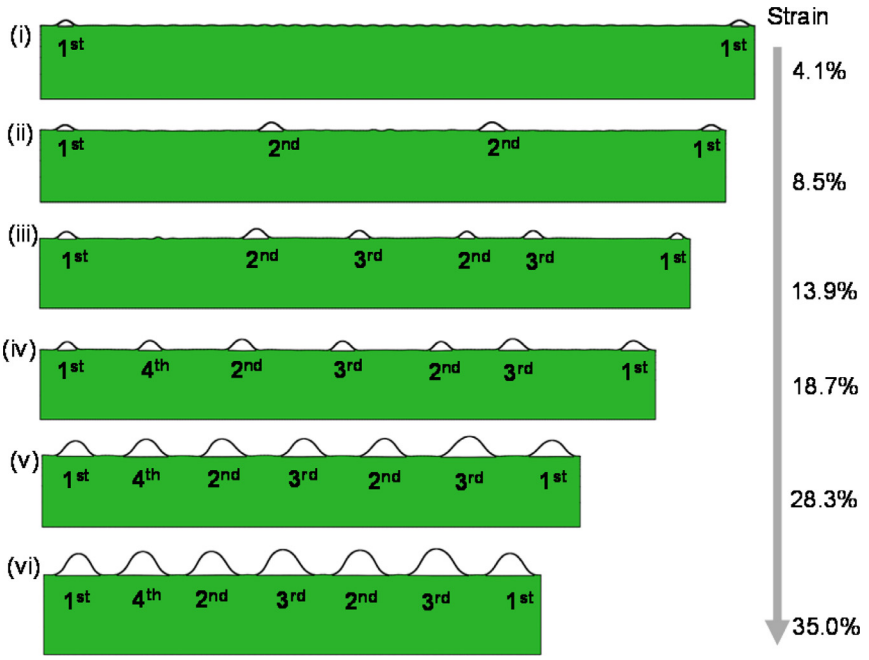

Fig. 8. FEM simulation results on the sequential formation and evolution of the macroscopic buckle-delamination of polymeric tape on silicone rubber substrates with the applied compression strain.

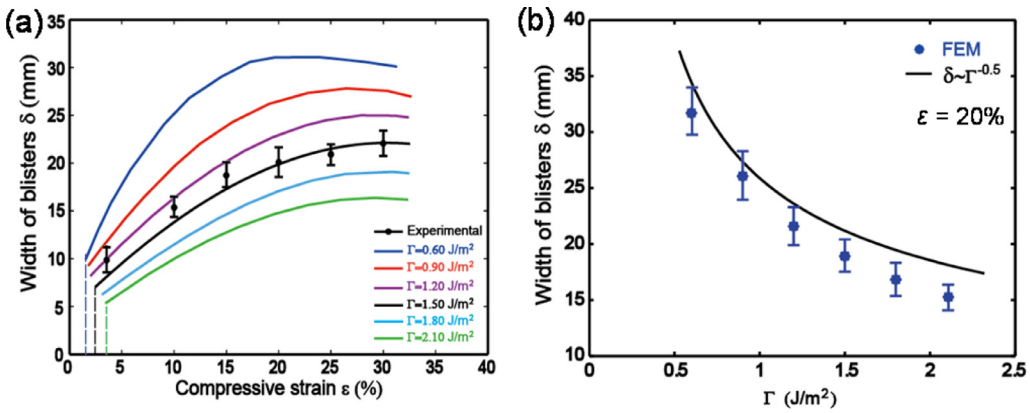

Fig. 9. (a) FEM simulation results on the effect of the interfacial toughness Γ on the blister width δ vs. applied compressive strain ε in the macroscopic buckle-delamination of polymeric tapes on silicone rubber substrates, and the comparison between the FEM simulation and experiment at $\Gamma = 1.5\,\mathrm{J/m^2}$. (b) Comparison between the FEM simulation and theoretical prediction of the width δ of macroscopic blisters as a function of the interfacial toughness Γ at $\varepsilon = 20\%$.

4.2. Effect of interfacial toughness Γ on the size of blisters

To investigate the effect of the interfacial toughness Γ on the size of the blisters, in the simulation, we set the value of Γ to increase from $0.6\,\mathrm{J/m^2}$ to $2.1\,\mathrm{J/m^2}$ to model the relatively weaker and stronger interfacial adhesion, respectively. Fig. 9a shows the average width of the blisters δ vs. the applied compressive strain ε for Γ changing from $0.6\,\mathrm{J/m^2}$ to $2.1\,\mathrm{J/m^2}$. It shows that δ increases nonlinearly with ε for all values of Γ. At $\Gamma = 1.5\,\mathrm{J/m^2}$, the simulated δ - ε curve agrees well with the experimental data on the size of the blisters. The starting point in each curve represents the onset of localized blisters. As Γ increases, we observe that the size of the first localized blisters reduces while the critical buckle-delamination strain ε_c increases, which is consistent with the theory discussed in Section 3.1. Fig. 9a also shows that at a given ε, the size of the blisters decreases with the increase of Γ.

Fig. 9b shows the simulated curve of blisters width δ as a function of the interfacial toughness Γ at $\varepsilon = 20\%$. It shows that δ decreases nonlinearly with Γ, which captures well with the theoretical prediction of $\delta \propto (\Gamma)^{-\frac{1}{2}}$ in Eq. (24) with all the other materials properties and film thickness being kept the same. It is observed that the theoretically predicted

δ is slightly higher than that in the simulation. The reason is that in the modeling, it assumes an idealized distribution of periodic sinusoidal blisters on the substrate, where a line bonding between the wave trough of the blisters. Thus, a negligible adhesion width with the substrate is assumed when compared to that of the blisters. However, as seen from the simulation in Fig. 8iv–vi, generally, when compared to the width of the blisters, the width of the bonded flat film between two neighboring blisters cannot be negligible, which gradually reduces with the increase of applied strain through the delamination crack propagation and is expected to become negligible at either a relatively larger applied strain or a weaker interfacial toughness. Thus, on average, the inextensibility assumption in modeling of the film will render a slightly larger δ than that from the FEM simulation. Furthermore, the disparity between the theory and FEM simulation is observed to grow with the increase of Γ at a given applied strain. This is reasonable since the increase in Γ leads to a higher energy barrier for the delamination crack to propagate, thus leading to an enlarging bonding width of the flat film between blisters, consequently, a smaller blister width in the simulation.

5. Potential implications in interfacial toughness measurement

Equipped with the theoretical modeling and FEM simulation on the buckle-delamination under large compression discussed above, next, we will first discuss the potential application of harnessing the information of periodic blisters' size for measurement of the interfacial toughness through our developed model discussed in Section 3.3 under large deformation. Similar implication is first discussed by Vella et al. (2009) in their study of macroscopic delamination of thin films on elastomers under small compression strain.

Typically, the interfacial toughness Γ is known as the required energy to separate the thin film and the substrate (Hutchinson and Suo, 1991; Volinsky et al., 2002), which remains challenging to be measured considering the micro/nanoscale thickness of the film. In most circumstances, the interfacial toughness is assumed to be equal to the true work of adhesion W_{ad}, i.e.

$$\Gamma = W_{ad} = \gamma_f + \gamma_s - \gamma_{fs} \tag{36}$$

where γ_f, γ_s, and γ_{fs} are the specific surface energies of the film and the substrate and the interface energy, respectively. For a given film/substrate system, the true work of adhesion is a constant. The most prevalent test to measure the interfacial toughness is the 90° peel test (Volinsky et al., 2002). This peel test is proceeded by measuring the required force P_f to pull off the film from the substrate. Assuming energy dissipation occurs in the interface without plasticity in the film, the energy-based failure criterion can be used to analyze this peel test. Therefore, according to the Kendall's peel test model (Kendall, 1975), the interfacial toughness can be expressed as

$$\Gamma = \frac{P_f^2}{2E_f w_b^2 t} + \frac{P_f}{w_b}(1 - \cos\theta) \tag{37}$$

where E_f, w_b, and t are the Young's modulus, the width, and the thickness of the film, respectively as defined before. Based on the peel test experiment, we measure the interfacial toughness between the 3 M scotch magic tapes (thickness $t = 50\,\mu m$) and the silicone rubber strips (thickness $t_s = 2\,mm$). From the load-crack length curve tested by the Instron microtester (Model 5944), for fixed peel angle $\theta = 90°$, the interfacial toughness is measured as $\Gamma \approx 1.5\,J/m^2$.

Alternatively, from Eq. (24), the interfacial toughness Γ can be estimated based on the dimension of the periodic delaminated blisters as below

$$\Gamma = \frac{\pi^2 \bar{E}_f t^3 \varepsilon}{\delta^2} \tag{38}$$

With the measured data in the macro-delamination experiment in Stage II, including the blister width δ and strain ε shown in Fig. 6a, the interfacial toughness Γ can be estimated as $\Gamma \approx 1.4 \pm 0.2\,J/m^2$ by fitting the experimental data in Eq. (38), which agrees well with the measurement through the peeling test.

6. Potential implication in design of extreme stretchable electronics

6.1. *Maximum tensile strain* ε_{max}

The strategy of buckling is widely used and explored in design of extreme stretchable electronics by bonding metal or semiconductor thin films to a pre-stretched soft elastomeric substrate electronics (Khang et al., 2006; Rogers et al., 2010; Yao and Zhu, 2015), where the accumulated strain in the thin film are effectively released through buckling upon pre-strain release. Normally, the crests of buckles are under tension and suffer the maximum tensile strain at the peak. When the maximum tensile strain ε_{max} is larger than the fracture strain of the constituent materials in the film $\varepsilon_{fracture}$, i.e. $\varepsilon_{max} \geq \varepsilon_{fracture}$, fracture occurs. Thus, the key in designing extremely stretchable electronics is to largely reduce ε_{max} through buckling to maximally release the strain energy. Here, we propose that compared to wrinkling without debonding, the spontaneous periodic buckle-delamination of stiff thin films on pre-strained soft substrates can relieve the accumulated strain energy in the film more effectively, and thus render a smaller ε_{max} to ensure a potential relatively larger stretchability.

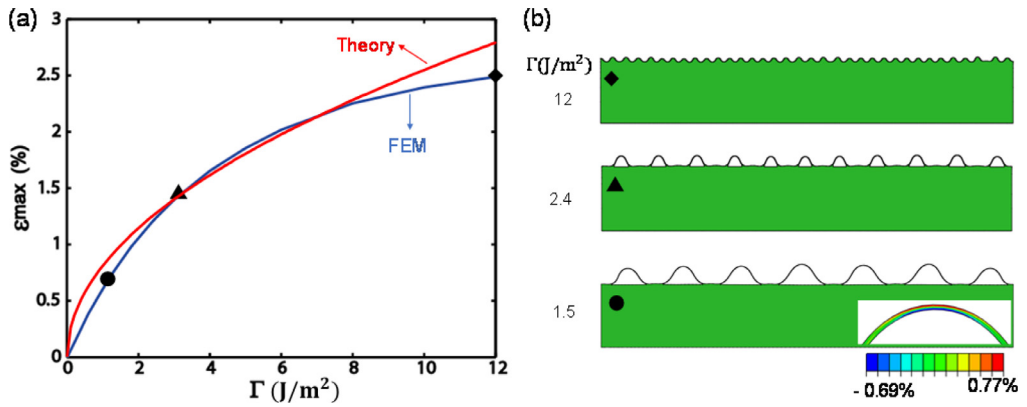

Fig. 10. (a) Comparison between FEM simulation and theoretical model on the effect of interfacial toughness Γ on the maximum tensile strain $\varepsilon_{\max}$ in the macroscopic buckle-delamination of polymeric tape strips on silicone rubber substrate at $\varepsilon = 30\%$. (b) The corresponding simulated buckled morphologies at different Γ, showing a transition from buckle-delamination to wrinkling as Γ increases from 1.5 J/m^2 to 12 J/m^2. The inset on the bottom shows the magnified strain contour of ε_{11}.

The maximum tensile strain in the buckled film is given by

$$\varepsilon_{\max} = \frac{t}{2R_c} \text{ with } R_c = \left| \frac{\left(1 + y'^2\right)^{3/2}}{y''} \right| \tag{39}$$

where R_c is the radius of curvature of a buckle (e.g. wrinkle or blister) at its crest and y is the function of the buckled profile.

For periodic buckle-delamination, if the geometrical profile of a blister can be approximated as a sinusoidal shape, we have $R_c = 1/y''$ at the crest of the blister with $y' = 0$. After substituting the sinusoidal function in Eq. (3) into Eq. (39), the maximum tensile strain $\varepsilon_{\max}$ in the periodic sinusoidal-like blisters can be calculated as

$$\varepsilon_{\max} = \frac{\pi^2 th}{\delta^2} = 2\sqrt{\frac{\Gamma}{\bar{E}_f t(1-\varepsilon)}} \tag{40}$$

with the help of Eqs. (24) and (25).

Similarly, if the geometrical profile of a blister can be approximated as a jig-saw-like or elastica shape, $\varepsilon_{\max}$ in the elastica blisters can be numerically obtained after submitting its profile functions of Eqs. (33) and (34) into Eq. (39) with the help of Eq. (35).

As seen from Eq. (40), for a given film-substrate system, the maximum tensile strain $\varepsilon_{\max}$ in the buckled film is mainly determined by the interfacial toughness Γ and the applied compression strain ε in the film, where Γ determines whether to wrinkle without debonding or delaminate, and ε determines the different delaminated profiles in a moderate or large compression strain range. Based on the simple model and FEM simulations, in the following, we will first discuss the potential benefit of buckle-delamination over wrinkling for achieving a relatively lower $\varepsilon_{\max}$ in the film (Section 6.2), then, we will discuss how the different buckle-delaminated shapes will influence $\varepsilon_{\max}$ in the film (Section 6.3).

6.2. ε_{max} in blisters vs. wrinkles: effect of Γ

Compared to wrinkling without debonding, we believe that the spontaneous periodic buckle-delamination could potentially release more strain energy through both buckling and delamination crack propagation, thus leading to a smaller ε_{max} in the delaminated film than that in the wrinkled film.

To validate that, we conduct a parametric study using FEM simulation to explore the maximum tensile strain ε_{max} in the buckled thin film as a function of the interfacial toughness Γ at the same applied compressive strain of $\varepsilon = 30\%$ as shown in Fig. 10a. The corresponding representative simulated buckled profiles of the thin film-substrate system at different Γ are shown in Fig. 10b. In the simulation, the same model system of polymeric tapes on the silicone rubber as that discussed in Section 4 is used. Fig. 10a shows that as Γ increases from 0 J/m^2 to 12 J/m^2, ε_{max} increases monotonically from 0 to 2.5%, which is in good agreement with the theoretical prediction from Eq. (40). However, a large disparity at $\Gamma = 12$ J/m^2 between the FEM and the model is observed due to the buckling mode transition from buckle-delamination to wrinkling as shown in Fig. 10b. Fig. 10b shows that as Γ gradually increases, the size of the periodic blisters reduces in both amplitude and width. However, when Γ reaches a larger value of 12 J/m^2, the periodic buckle-delamination transits to wrinkling without debonding from the substrate, which accounts for the observed discrepancy in the model. We find that $\varepsilon_{\max}$ in the wrinkled film reaches 2.5%, which is over 3 times larger than that in the buckle-delaminated film at $\Gamma = 1.5$ J/m^2

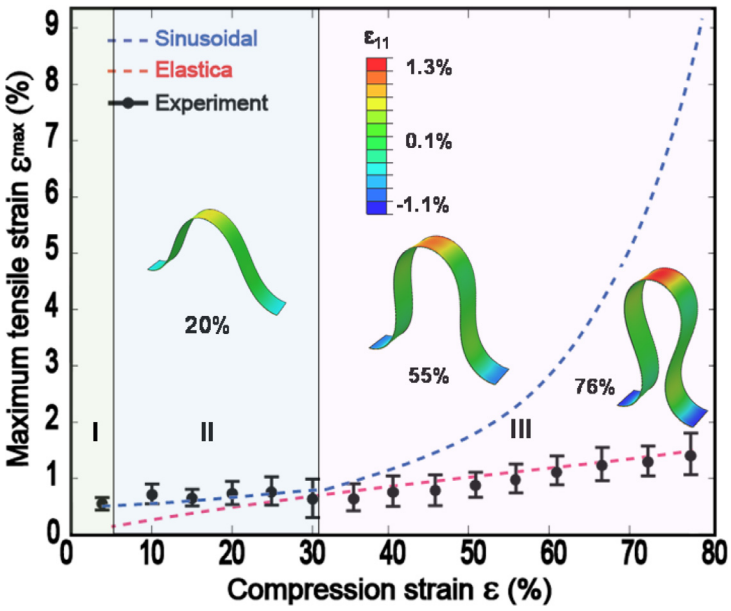

Fig. 11. Comparison between the theoretical prediction and experimental measurement on the maximum tensile strain $\varepsilon_{\max}$ in the macroscopic buckle-delaminated tape stripes on silicone rubber substrate as a function of the compressive strain ε. The blister takes either an assumed sinusoidal shape (blue dashed curve) or an elastica shape (red dashed curve) throughout the increase of ε. Insets are the FEM simulation results on the evolution of buckled shapes of a polymeric tape strip with the end-to-end compression. (For interpretation of the references to color in this figure legend, the reader is referred to the web version of this article.)

($\varepsilon_{\max} = 0.77\%$ located on the crest of the blister as shown in the strain contour of Fig. 10), thus showing the potential benefit of buckle-delamination over wrinkling in lowering the peak strain in the buckled film.

6.3. ε_{max} in sinusoidal-shaped vs. elastica blisters: effect of ε

To explore how the different buckle-delaminated shapes influence the value of $\varepsilon_{\max}$ during the spontaneous periodic buckle-delamination, we assume that in the macro-delamination experiment discussed in Section 2.2, the growing blisters always take either an approximately sinusoidal or an elastica profile throughout the whole large pre-strain release and compression process.

Fig. 11 shows the comparison of the theoretically predicted $\varepsilon_{\max}$ between the assumed sinusoidal and elastica-shaped blisters in the buckle-delaminated tape. It shows that generally the sinusoidal blisters exhibit a higher value of $\varepsilon_{\max}$ than the elastica blisters. As ε increases, $\varepsilon_{\max}$ grows parabolically in the sinusoidal-shaped blisters while approximately linearly in the elastica blisters. Specifically, within the small and moderate compression strain range, i.e. $5\% \le \varepsilon \le 31\%$ in Stage II, $\varepsilon_{\max}$ in the sinusoidal-shaped blisters is slightly higher than that in the elastica blisters, however, as ε further increases to the large and even extremely large compression strain range, i.e. $31\% \le \varepsilon \le 80\%$ in Stage III, $\varepsilon_{\max}$ in the sinusoidal blister grows dramatically to be significantly higher than that in the elastica blister despite its similar amplitude and width (Fig. 7b). Thus, it implies that compared to the sinusoidal shape, the elastica blister can release the strain energy more effectively to render a relatively smaller peak strain in the film, especially at large compression strain, which explains why there is a shape transition of the blisters observed in experiments when beyond the transition strain ε_T. Fig. 11 also shows that the theoretical models of combining the sinusoidal shape in Stage II and elastica shape in Stage III agree well with the experimental measurement, which validates the theoretical prediction. We find that at an extremely large compressive strain of close to 80%, corresponding to a pre-stretched strain of close to 400% in the substrate, the maximum tensile strain $\varepsilon_{\max}$ in the buckle-delaminated tape is only $1.2 \pm 0.2\%$, which is over 300 times smaller than the substrate pre-strain.

The small peak strain in the buckled elastica blisters in Stage III of large compressive strain is further validated by the corresponding FEM simulation. Since there is no adhesive energy releasing between the thin film and the substrate in Stage III, in the simulation, we only consider the deformation of the thin film. The stiff thin film is modeled as a layer of 4-noded shell elements and is compressed horizontally through a displacement loading on its two ends, where the vertical displacement and the rotation are constrained at its two ends. The length of the modeled thin film is set to be equal to the arc length of one blister which is determined based on the calculation at $\Gamma = 1.5\,\mathrm{J/m^2}$ in Stage II. The simulation results of the normal strain ε_{11} in the buckled blister are shown in the inset of Fig. 11. It shows that as ε increases, the buckled blister exhibits an elastica profile with $\varepsilon_{\max}$ located on its crest. When ε reaches 76%, a maximum tensile strain of 1.3% is observed in the simulation, which agrees well with both experimental and theoretical results.

7. Conclusion

In conclusion, through a combined experiment, theoretical modeling, and FEM simulation, we explored the mechanics governing the formation and evolution of spontaneous buckling-driven periodic delamination of thin films on largely pre-strained soft substrates, as well as its potential applications in interfacial toughness measurement and potential design of extremely stretchable electronics.

Based on the experimental observation of morphological transition in the periodic blisters from a sinusoidal to an elastica profile, we developed an energy-minimization based three-stage theoretical model to investigate the formation (Stage I), growth (Stage II), and shape transition and evolution (Stage III) of the buckle-delaminated blisters under applied large compression strain. The respective model governing the geometry of the blisters in each stage is validated by the experiments and FEM simulations. Based on the validated model, we proposed a simple method for measuring the interfacial toughness through the metrology of periodic blisters. Lastly, we validated that the spontaneous periodic buckle-delamination can release more strain energy than wrinkling to render a smaller maximum tensile strain in the buckled film. Under large compression, elastica blisters present a much smaller maximum tensile strain than that of sinusoidal blisters. The results of this study could find potential applications in design of extremely stretchable electronics through spontaneous periodic buckle-delamination. The high-aspect-ratio features and jig-saw-like shapes on the microscale periodic delamination could find potential applications in exploring the uniqueness in high-aspect-ratio surface related properties in wetting, optics, adhesion, and anti-icing etc.

Acknowledgment

J.Y. acknowledges the funding support from the National Science Foundation (NSF) (CMMI-1727792).

References

Audoly, B., 1999. Stability of straight delamination blisters. Phys. Rev. Lett. 83, 4124–4127.
Audoly, B., Boudaoud, A., 2008. Buckling of a thin film bound to a compliant substrate- partII: a global scenario for the formation of herringbone pattern. J. Mech. Phys. Solids 56, 2422–2443.
Bae, H.J., Bae, S., Park, C., Han, S., Kim, J., Kim, L.N., Kim, K., Song, S.-H., Park, W., Kwon, S., 2015. Biomimetic microfingerprints for anti-counterfeiting strategies. Adv. Mater. 27, 2083–2089.
Bowden, N., Brittain, S., Evans, A.G., Hutchinson, J.W., Whitesides, G.M., 1998. Spontaneous formation of ordered structures in thin films of metals supported on an elastomeric polymer. Nature 393, 146.
Brau, F., Vandeparre, H., Sabbah, A., Poulard, C., Boudaoud, A., Damman, P., 2010. Multiple-length-scale elastic instability mimics parametric resonance of nonlinear oscillators. Nat. Phys. 7, 56.
Breid, D., Crosby, A.J., 2011. Effect of stress state on wrinkle morphology. Soft Matter 7, 4490–4496.
Cai, S., Breid, D., Crosby, A.J., Suo, Z., Hutchinson, J.W., 2011. Periodic patterns and energy states of buckled films on compliant substrates. J. Mech. Phys. Solids 59, 1094–1114.
Chen, X., Hutchinson, J.W., 2004. Herringbone buckling patterns of compressed thin films on compliant substrates. J. Appl. Mech. 71, 597–603.
Chen, Y.-C., Crosby, A.J., 2014. High aspect ratio wrinkles via substrate prestretch. Adv. Mater. 26, 5626–5631.
Chung, J.Y., Nolte, A.J., Stafford, C.M., 2011. Surface wrinkling: a versatile platform for measuring thin-film properties. Adv. Mater. 23, 349–368.
Ebata, Y., Croll, A.B., Crosby, A.J., 2012. Wrinkling and strain localizations in polymer thin films. Soft Matter 8, 9086–9091.
Efimenko, K., Finlay, J., Callow, M.E., Callow, J.A., Genzer, J., 2009. Development and Testing of hierarchically wrinkled coatings for marine antifouling. ACS Appl. Mater. Interfaces 1, 1031–1040.
Gioia, G., Ortiz, M., 1997. Delamination of compressed thin films. Adv. Appl. Mech. 33, 119–192.
Huang, R., Suo, Z., 2002. Wrinkling of a compressed elastic film on a viscous layer. J. Appl. Phys. 91, 1135–1142.
Huang, Z.Y., Hong, W., Suo, Z., 2005. Nonlinear analyses of wrinkles in a film bonded to a compliant substrate. J. Mech. Phys. Solids 53, 2101–2118.
Humer, A., Irschik, H., 2011. Large deformation and stability of an extensible elastica with an unknown length. Int. J. Solids Struct. 48, 1301–1310.
Hutchinson, J.W., Suo, Z., 1991. Mixed mode cracking in layered materials. Adv. Appl. Mech. 29, 63–191.
Hutchinson, J.W., Thouless, M.D., Liniger, E.G., 1992. Growth and configurational stability of circular, buckling-driven film delaminations. Acta Metall. Mater. 40, 295–308.
Hutchinson, J.W., Suo, Z., 1992. Mixed mode cracking in layered materials. Adv. Appl. Mech. 29, 63–191.
Jensen, H., Sheinman, I., 2001. Straight-sided, buckling-driven delamination of thin films at high stress levels. Int. J. Fract. 110, 371–385.
Jiang, H., Khang, D.-Y., Song, J., Sun, Y., Huang, Y., Rogers, J.A., 2007. Finite deformation mechanics in buckled thin films on compliant supports. Proc. Natl. Acad. Sci. 104, 15607–15612.
Kendall, K., 1975. Thin-film peeling-the elastic term. J. Phys. D Appl. Phys. 8, 1449.
Khang, D.-Y., Jiang, H., Huang, Y., Rogers, J.A., 2006. A stretchable form of single-crystal silicon for high-performance electronics on rubber substrates. Science 311, 208–212.
Lee, E., Zhang, M., Cho, Y., Cui, Y., Van der Spiegel, J., Engheta, N., Yang, S., 2014. Tilted pillars on wrinkled elastomers as a reversibly tunable optical window. Adv. Mater. 26, 4127–4133.
Lee, S.G., Lee, D.Y., Lim, H.S., Lee, D.H., Lee, S., Cho, K., 2010. Switchable transparency and wetting of elastomeric smart windows. Adv. Mater. 22, 5013–5017.
Lin, G., Chandrasekaran, P., Lv, C., Zhang, Q., Tang, Y., Han, L., Yin, J., 2017. Self-similar hierarchical wrinkles as a potential multifunctional smart window with simultaneously tunable transparency, structural color, and droplet transport. ACS Appl. Mater. Interfaces 9, 26510–26517.
Love, A.E.H., 1906. A Treatise on the Mathematical Thoery of Elasticity. The University Press.
Mei, H., Huang, R., Chung, J.Y., Stafford, C.M., Yu, H.-H., 2007. Buckling modes of elastic thin films on elastic substrates. Appl. Phys. Lett. 90, 151902.
Mei, H., Landis, C.M., Huang, R., 2011. Concomitant wrinkling and buckle-delamination of elastic thin films on compliant substrates. Mech. Mater. 43, 627–642.
Moon, M.-W., 2013. Buckling delamination of compressed thin films. In: Chen, X. (Ed.), Mechanical Self-Assembly. Springer, New York, pp. 131–152.
Moon, M.W., Jensen, H.M., Hutchinson, J.W., Oh, K.H., Evans, A.G., 2002. The characterization of telephone cord buckling of compressed thin films on substrates. J. Mech. Phys. Solids 50, 2355–2377.
Ohzono, T., Suzuki, K., Yamaguchi, T., Fukuda, N., 2013. Tunable optical diffuser based on deformable wrinkles. Adv. Opt. Mater. 1, 374–380.
Ortiz, M., Gioia, G., 1994. The morphology and folding patterns of buckling-driven thin-film blisters. J. Mech. Phys. Solids 42, 531–559.
Ortiz, M., Gioia, G., 1997. Delamination of compressed thin films. Adv. Appl. Mech. 33, 119–192.

Rahmawan, Y., Chen, C.-M., Yang, S., 2014. Recent advances in wrinkle-based dry adhesion. Soft Matter. 10, 5028–5039.
Rogers, J.A., Someya, T., Huang, Y., 2010. Materials and mechanics for stretchable electronics. Science 327, 1603–1607.
Rudykh, S., Boyce, M.C., 2014. Transforming wave propagation in layered media via instability-induced interfacial wrinkling. Phys. Rev. Lett. 112, 034301.
Saif, M.T.A., 2000. On a tunable bistable MEMS-theory and experiment. J. Microelectromech. Syst. 9, 157–170.
Song, J., Jiang, H., Liu, Z.J., Khang, D.Y., Huang, Y., Rogers, J.A., Lu, C., Koh, C.G., 2008. Buckling of a stiff thin film on a compliant substrate in large deformation. Int. J. Solids Struct. 45, 3107–3121.
Sun, Y., Choi, W.M., Jiang, H., Huang, Y.Y., Rogers, J.A., 2006. Controlled buckling of semiconductor nanoribbons for stretchable electronics. Nat. Nano 1, 201–207.
Thomas, A.V., Andow, B.C., Suresh, S., Eksik, O., Yin, J., Dyson, A.H., Koratkar, N., 2015. Controlled crumpling of graphene oxide films for tunable optical transmittance. Adv. Mater. 27, 3256–3265.
Timoshenko, S.P., Gere, J.M., 1961. Theory of Elastic Stability. McGraw-Hill, New York.
Vella, D., Bico, J., Boudaoud, A., Roman, B., Reis, P.M., 2009. The macroscopic delamination of thin films from elastic substrates. Proc. Natl. Acad. Sci. 106, 10901–10906.
Volinsky, A.A., Moody, N.R., Gerberich, W.W., 2002. Interfacial toughness measurements for thin films on substrates. Acta Mater. 50, 441–466.
Wagner, T.J.W., Vella, D., 2013. The 'sticky elastica': delamination blisters beyond small deformations. Soft Matter. 9, 1025–1030.
Wang, Q., Zhao, X., 2015. A three-dimensional phase diagram of growth-induced surface instabilities. Sci. Rep. 5, 8887.
Yao, S., Zhu, Y., 2015. Nanomaterial-enabled stretchable conductors: strategies. Mater. Dev. Adv. Mater. 27, 1480–1511.
Yin, J., Boyce, M.C., 2015. Materials science: unique wrinkles as identity tags. Nature 520, 164–165.
Yin, J., Chen, X., Sheinman, I., 2009. Anisotropic buckling patterns in spheroidal film/substrate systems and their implications in some natural and biological systems. J. Mech. Phys. Solids 57, 1470–1484.
Zang, J., Ryu, S., Pugno, N., Wang, Q., Tu, Q., Buehler, M.J., Zhao, X., 2013. Multifunctionality and control of the crumpling and unfolding of large-area graphene. Nat. Mater. 12, 321–325.
Zhang, Q., Tang, Y., Hajfathalian, M., Chen, C., Turner, K.T., Dikin, D.A., Lin, G., Yin, J., 2017. Spontaneous periodic delamination of thin films to form crack-free metal and silicon ribbons with high stretchability. ACS Appl. Mater. Interfaces 9, 44938–44947.